Control and Entanglement of Individual Rydberg Atoms near a Nanoscale Device

Paloma L. Ocola,[1,*] Ivana Dimitrova,[1,*] Brandon Grinkemeyer,[1,*] Elmer Guardado-Sanchez,[1,*] Tamara Đorđević,[1] Polnop Samutpraphoot,[1] Vladan Vuletić,[2] and Mikhail D. Lukin[1,†]

[1]*Department of Physics, Harvard University, Cambridge, Massachusetts 02138, USA*
[2]*Massachusetts Institute of Technology, Cambridge, Massachusetts 02139, USA*

(Received 2 November 2022; revised 10 May 2023; accepted 23 January 2024; published 14 March 2024)

Coherent control of Rydberg atoms near dielectric surfaces is a major challenge due to the large sensitivity of Rydberg states to electric fields. We demonstrate coherent single-atom operations and two-qubit entanglement as close as 100 μm from a nanophotonic device. Using the individual atom control enabled by optical tweezers to study the spatial and temporal properties of the electric field from the surface, we employ dynamical decoupling techniques to characterize and cancel the electric-field noise with submicrosecond temporal resolution. We further use entanglement-assisted sensing to accurately map magnitude and direction of electric-field gradients on a micrometer scale. Our observations open a path for integration of Rydberg arrays with micro- and nanoscale devices for applications in quantum networking and quantum information science.

DOI: 10.1103/PhysRevLett.132.113601

Significant progress is currently being made in developing quantum information processors across a variety of different physical platforms [1]. Further increasing the computational power may require connecting multiple processors via quantum interconnects [2]. In particular, Rydberg atom arrays have recently emerged as a leading platform for quantum simulations and quantum information processing [3–5]. While scaling to many thousands of controlled qubits appears feasible [6], significant advances can be achieved by coupling Rydberg arrays to optical, microwave, and electronic devices. Integration with these devices could enable quantum networking via optical photons [7–11], as well as novel coupling and control techniques via microwave photons [12]. However, in practice, Rydberg qubits experience decoherence near surfaces caused by fluctuating charges.

Over the past decade, coherent excitation to Rydberg states in atomic gases has been achieved near various types of surfaces, including glass [13], quartz [14], inside hollow-core fibers [15], an optical nanofiber [16], atom chips [17–19], and superconducting surfaces [20–22]. Compensation for the stray electric fields, in part caused by alkali adsorption on these surfaces, has been approached through light-induced desorption [18,19], heating of the surfaces [13,14,21], applying in-vacuum electric fields [17,22], or deposition of a thin metallic alkali layer [20]. However, quantum information applications often require understanding and control of local electric fields at micrometer scales with submicrosecond temporal resolution that cannot be obtained using sensing with macroscopic atom samples.

In this Letter, we leverage the control over individual atom qubits trapped in moveable optical tweezers to study in detail the spatial and temporal properties of electric fields from a dielectric surface. Specifically, we experimentally demonstrate coherent control of individual Rydberg qubits and entanglement of qubit pairs in close proximity to a nanoscale photonic device made of silicon nitride, used previously to achieve atom-photon and transportable atom-atom entanglement [23,24]. The effects of stray electric fields are minimized by using a small-surface area device and illuminating it with UV light at an optimized power. Remarkably, we find that the electric field from the device resembles a point charge of ∼200 single electron charges (e) with quasistatic fluctuations. This enables coherent control via decoupling pulse sequences at distances as close as 100 μm from the device. Moreover, we demonstrate that the electric-field noise from the device surface minimally perturbs a two-atom entangled state at these distances. This allows us to map the local electric-field gradient by changing the relative orientation of the two entangled atoms, realizing an entanglement-assisted measurement, based on a decoherence-free subspace. Two-qubit spin echo-based and entanglement-assisted measurements are being actively explored in systems involving individual color centers [25–28], trapped ions [29–33], and atoms [34,35]. Here, these approaches are applied to individual neutral atoms in optical tweezers, enabling novel types of local electrical noise measurements. Together with the recently demonstrated coherent transport of ground state atoms [24,36], our observations pave the way for integrating Rydberg arrays with micro- and nanoscale devices.

In our experiments, individual Rubidium-87 atoms are loaded in optical tweezers from a magneto-optical trap. The experiment begins when magneto-optical trap light scattered by the atom is collected via the optical tweezer path to indicate atomic presence, which allows us to select for

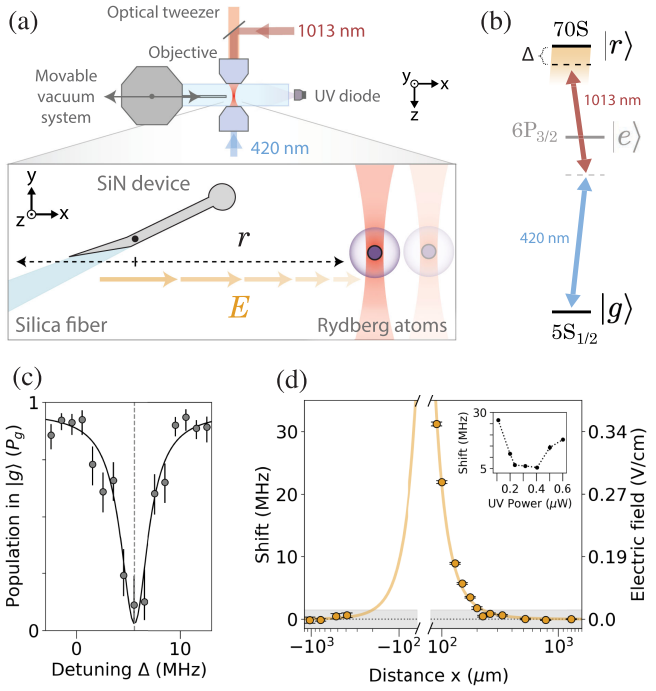

FIG. 1. Rydberg spectral shift. (a) Experimental setup. (b) Two-photon excitation to the Rydberg state, which is shifted by electric fields (yellow shade). (c) Ground state population P_g as a function of the two-photon detuning Δ at 150 μm from the device, where the spectrum center (dashed line) is determined via a Lorentzian fit (black line). (d) Measured spectral shift as a function of distance from the device fitted to a point-charge model (yellow line, Supplemental Material [37], Sec. 2.1). The shift only exceeds the Rabi-broadened linewidth (shaded gray region) for distances less than 250 μm. Inset: spectral shift dependence on UV power at 160 μm.

experiments of either one or two atoms. The device is suspended on a tapered silica fiber connected to a translation stage [Fig. 1(a)], allowing it to be positioned 90–2600 μm from the trapped atoms. Each atom is prepared in $|g\rangle = |5S_{1/2}, F = 2, m_F = 2\rangle$ and excited to the $|r\rangle = |70S_{1/2}, m_J = 1/2\rangle$ Rydberg state via a two-photon transition [Fig. 1(b)]. Atoms in the Rydberg state in our system are repelled by the tweezer light. While this requires the tweezer light to be pulsed off during experiments, turning the tweezer back on removes the population in the Rydberg state. Therefore, in subsequent fluorescence imaging, Rydberg population is signaled via atom loss.

The Rydberg state in an electric-field $\mathbf{E}$ experiences a Stark shift $\Delta\nu = \frac{1}{2}\alpha|\mathbf{E}|^2$ [41], with polarizability $\alpha = 534\ \mathrm{MHz/(V/cm)^2}$ [42]. Its spectral shift is measured by exciting the atom and varying the detuning of the 420 nm light in the two-photon transition to take a spectrum [Fig. 1(c)]. Each detuning data point of the spectrum is averaged over multiple experimental runs with single atoms. The shift follows the electric-field scaling of a point charge (r^{-4}) located on the 31.5 μm-long device [Fig. 1(d)]. Assuming the charge is at the center of the device, a fit gives an estimated charge $q = 126(11)$ e (Supplemental Material [37], Sec. 2). As discussed below, at each distance the shift is minimized by illuminating the experimental setup with a UV diode and optimizing its power [Fig. 1(d), inset]. Furthermore, the spectral shift is stable only with a relatively constant rate of Rydberg excitation, interpreted as Rydberg-atom ionization creating charges that neutralize the device surface. Similar effects were observed in Rydberg electromagnetically-induced-transparency experiments near a quartz surface [14]. The Rydberg spectral shift can be stabilized via both effects as close as 90 μm to the device (Supplemental Material [37], Sec. 3).

The temporal properties of the electric field from the device are probed by measuring the coherence of the ground-Rydberg qubit with various control sequences. By pulsing the 420 nm light, we apply a Ramsey sequence to extract T_2^* as a function of distance from the device [Fig. 2(a)]. With an echo pulse sequence [Fig. 2(b)], the coherence time is extended by nearly an order of magnitude. Extending to a Carr-Purcell (CP) $N = 2$ decoupling sequence [Fig. 2(c)], no decay is observed within the 10 μs evolution time at any measured distance. This implies that the electric-field noise is quasistatic: stable within a single realization. We construct a model for the decoherence that includes a point-charge electric field from the device that

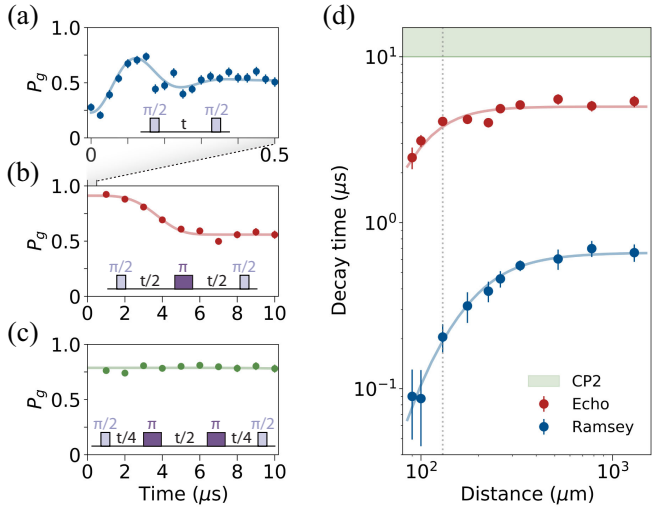

FIG. 2. Ground-Rydberg qubit coherence. Ground state population P_g as measured after a Ramsey (a), spin-echo (b), and Carr-Purcell (CP) $N = 2$ (c) pulse sequences at 130 μm [dotted line in (d)]. A decaying sinusoid fit (blue line) gives $T_2^* = 200(40)$ ns and a Gaussian decay function (red line) gives $T_2 = 4.1(2)$ μs. The CP $N = 2$ data exhibits no decay within the measurement time. (d) Measured T_2 (red circles) and T_2^* (blue circles) as a function of distance from the device. The solid lines are fits to the data given our decoherence model (Supplement Material [37], Sec. 4). The shaded green region is a lower bound on the CP $N = 2$ coherence time.

scales with distance and a background electric field that does not, both of which vary between experimental realizations. The standard deviation of each can be extracted by fitting the distance scaling of T_2 and T_2^* [Fig. 2(d)]. We determine a background field $|E| = 0.367$ V/cm with fluctuation of 0.012 V/cm and a fluctuation of charges on the device ≤ 8 e. Our model implies that T_2^* is limited by the electric-field fluctuations, primarily from the background field, and that T_2 is limited by thermal sampling of the spatially dependent electric field (Supplemental Material [37], Sec. 4). Therefore, by applying decoupling sequences coherent Rydberg manipulations can be performed as close as the range 100–300 μm, which is traversable using commercial microscope objectives [36].

We next prepare and study entangled atom pairs at various distances from the device. Two atoms 3.15 μm apart experience a Rydberg-Rydberg interaction U in the blockade regime where $U \gg \Omega$, with $U \approx 2\pi \times 685$ Mhz and the single-atom Rabi frequency $\Omega \approx 2\pi \times 3$ MHz. The atoms are driven with a π pulse from $|gg\rangle$ into the symmetric state $|W\rangle = (1/\sqrt{2})(|gr\rangle + |rg\rangle)$ [Fig. 3(a)]. The preparation fidelity $\mathcal{F} = \frac{1}{2}(\rho_{rg,rg} + \rho_{gr,gr} + 2|\rho_{gr,rg}|)$

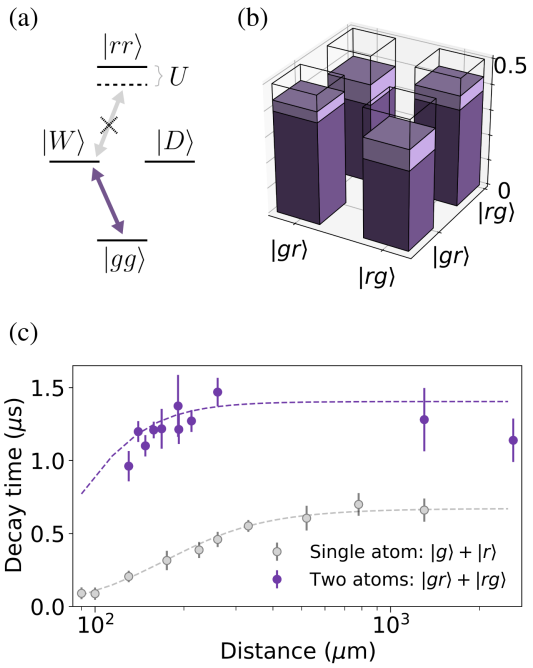

FIG. 3. Two-atom entangled state. (a) The Rydberg interaction U shifts the $|rr\rangle$ state and allows the preparation of the $|W\rangle = (1/\sqrt{2})(|gr\rangle + |rg\rangle)$ state. (b) Tomography of the $|W\rangle$ state (purple) at 170 μm. We measure population $\rho_{rg,rg} + \rho_{gr,gr} = 0.87(5)$ and coherence $2|\rho_{gr,rg}| = 0.78(7)$ with correction for preparation error and loss (light purple). (c) Comparison between the two-atom $|W\rangle$ state lifetime T_W (purple circles) and the single-atom ground-Rydberg coherence time T_2^* {gray circles, data and fit from [Fig. 2(d)]}. The dotted purple line is a theoretical prediction (Supplemental Material [37], Sec. 5.4).

is characterized following the method in [43] and corrected for error and loss during preparation. Far from the device at 2.6 mm it is 0.87(6) [uncorrected 0.73(3)] and remains similar close to the device: 0.83(4) [uncorrected 0.70(3)] at 170 μm [Fig. 3(b)].

The lifetime of the $|W\rangle$ state T_W is measured through a pulse sequence $\pi - t - \pi$ between the $|gg\rangle$ and $|W\rangle$. Compared to the single-atom ground-Rydberg coherence, T_W remains constant up to 130 μm since the electric-field fluctuations are common-mode for the two closely spaced atoms [Fig. 3(c)]. T_W is likely limited by thermal position sampling of the electric-field gradient, as supported by a theoretical model that only includes atomic temperature as a free parameter (Supplemental Material [37], Sec. 5).

The $|W\rangle$ state can be used to probe small electric field gradients within the blockade radius. The electric-field gradient creates an energy difference between $|gr\rangle$ and $|rg\rangle$ and thus a differential phase, leading to an oscillation between $|W\rangle$ and the antisymmetric state $|D\rangle = (1/\sqrt{2})(|gr\rangle - |rg\rangle)$. The oscillation frequency, observed via the $\pi - t - \pi$ pulse sequence, is proportional to the gradient magnitude. The minimum detectable frequency is $1/T_W$ and directly limits the minimum detectable electric-field gradient, which is ~ 10 V/cm^2 for the distances studied here (Supplemental Material [37], Sec. 6.4). By contrast, a measurement involving two individual atoms in different experimental realizations for each atom is limited by the electric-field fluctuations. For these reasons, the minimum detectable electric-field gradient for an entangled pair is higher by the ratio T_W/T_2^*, which is approximately 5 at 150 μm.

By rotating the entangled atom pair by an angle θ with respect to the x axis, the direction of maximum gradient can be detected via the oscillations induced in the lifetime measurement [Figs. 4(a) and 4(b)]. We perform measurements at four distances between 130 and 192 μm, the gradient maximum occurs at $\theta \sim 55°$ for each and its magnitude increases as the atoms approach the device [Fig. 4(c)]. This differs from the expected 0° gradient orientation for a single point charge displaced in x, but can instead be described by a minimal model that includes a distance-independent background electric field. A combined fit to the data in [Fig. 4(c)] reveals a device charge $q = 190(10)$ e and background field $\mathbf{E} = (E_x, E_y) = [-0.02(1), -0.51(3)]$ V/cm. The oscillation frequency follows the point-charge gradient scaling of r^{-5} along $\theta = 0°$ as well as r^{-3} along $\theta = 90°$, justifying the point-charge model. Together with the single-atom Rydberg spectral shifts, this measurement allows us to create a 2D map of the local electric field shown in Fig. 4(e) (Supplemental Material [37], Sec. 6). Going further, such maps of the local electric field can be used to study the charge characteristics of different materials that could be integrated with Rydberg atom arrays.

In particular, this measurement can be used to study the effect of UV light on the surfaces present. Many recent

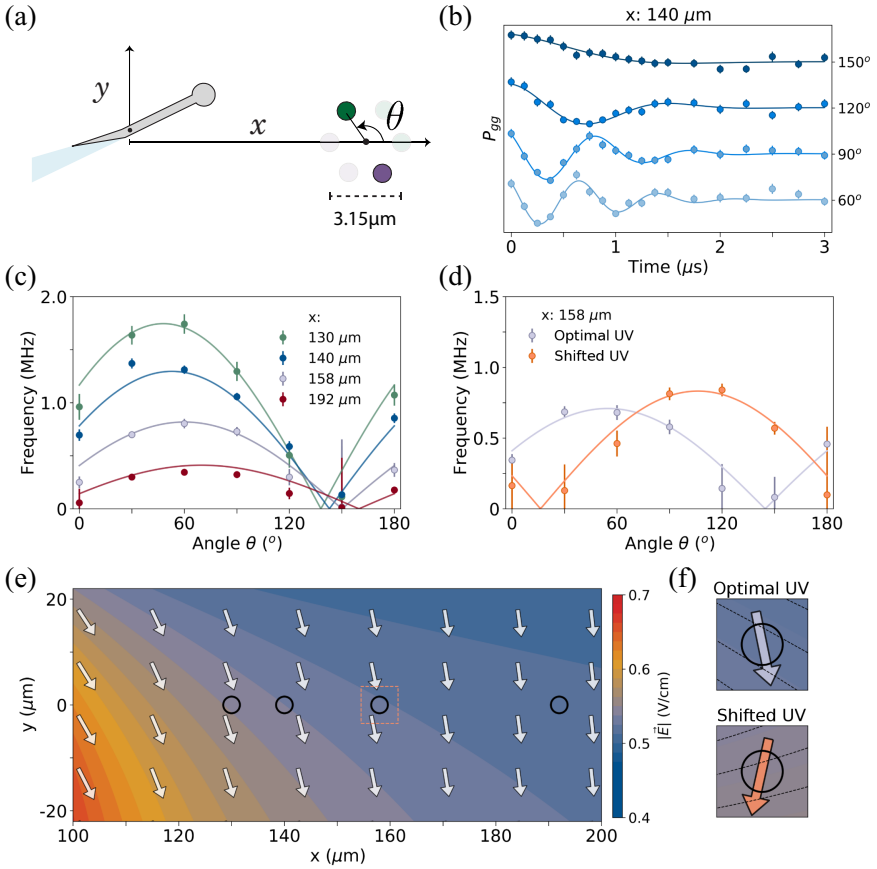

FIG. 4. Entanglement-assisted sensing of electric-field gradients. (a) The orientation of an entangled atom pair is varied with respect to the device. (b) The $|W\rangle$ state lifetime measurement (blue circles) reveals gradient-induced oscillations by fitting to a decaying sinusoid (blue lines) for different θ (offset for clarity). (c) Angular dependence of the fitted oscillation frequency at different x (circles) with solid curves being simultaneous fit (Supplemental Material [37], Sec. 6) to extract background field orientation. (d) A 200 nW UV-power reduction from its optimized value causes a rotation (53°) of the gradient. (e) Reconstructed electric-field magnitude $|\vec{E}|$ (contour scale) and direction (white arrows) given the measurements in (c) at the positions of the black circles. (f) Electric-field contour plot reconstructed from (d) showing direction at the optimal UV value (gray arrow) and shifted UV value (orange arrow).

Rydberg atom array experiments use ∼1 W of UV light to mitigate electric-field noise [43,44], with the current microscopic understanding that light-induced desorption of alkali atoms decreases the number of charges on dielectric surfaces [14,18,45]. Here, we observe that much smaller UV powers significantly affect the electric-field environment [Fig. 1(c), inset]. At 158 μm, decreasing the UV power from the optimal value of 400 to 200 nW increases the spectral shift by 6.7 MHz and rotates the gradient by 53(4)° [Fig. 4(d)]. Assuming the UV power change modifies the fit parameters q, E_x, E_y from Fig. 4(c), we reconstruct the changed electric field Fig. 4(f)]. We find a significant change only in the background electric field: $\Delta E_x = -0.21(3)$ V/cm and not in the charge on the device q (Supplemental Material [37], Sec. 6.5). However, we observe that far from the device, the background electric field sensed by the atom does not vary with UV power (Supplemental Material [37], Sec. 3.1).

One way of reconciling our observations is that another surface that moves with the device could be causing the shift in the background electric field, such as the tapered fiber. The minimization of the spectral shift using UV light could then be interpreted as the elimination of charges on the fiber surface. In fact, at the optimum UV power we do not observe any significant charges on the fiber, as indicated by the zero shift at negative x distances where the atom is much closer to the fiber surface than to the device [Fig. 1(d)]. By contrast, for large UV powers (∼30 mW) we find that the Rydberg spectral shift increases dramatically (Supplemental Material [37], Sec. 3.1). This behavior cannot be explained by the common understanding that higher UV power increases the removal rate of adsorbates and further work is needed to develop a full microscopic understanding. Remarkably, by choosing the optimum UV power, we repeatedly stabilize to the same charge configuration as indicated by measurements of the spectral shift (Supplemental Material [37], Sec. 3.3). Finally, while potential improvements to our device include minimizing its surface area and adding in-vacuum electrodes, significant enhancement can be achieved in the current

system by lowering the principal quantum number n to balance the Rydberg interaction strength with electric-field sensitivity (Supplemental Material [37], Sec. 7).

Our observations indicate that a Rydberg atom array placed ∼250 μm away would remain minimally perturbed by the nanophotonic device. This could be used to establish a quantum optical channel via teleportation to a photonic state [46], or to a distant quantum processor. A ground-state atom can be entangled with a photon at the device [23,47], and then coherently transported with a single tweezer to the atom array [24,36]. The transported atom can then be entangled with the Rydberg-atom quantum processor. Further, such optical interfaces can also be utilized for fast, nondestructive readout in quantum error correction protocols [48,49]. More broadly, our work motivates the integration of Rydberg atom arrays with other devices of this scale and could provide a helpful understanding for other platforms sensitive to surface charges [1]. For example, with properly designed decoupling sequences and charge stabilization, integration with a mesoscopic superconducting interface is possible, enabling the application of circuit QED techniques and exploration of novel hybrid systems [12,50–52].

We thank S. Ebadi, T. T. Wang, D. Bluvstein, T. Manovitz, G. Semeghini, and S. Evered for useful discussions, technical assistance, and sharing of laser light. We also acknowledge M. Greiner, R. Riedinger, and H. R. Sadeghpour for insightful discussions. This work was supported by the Center for Ultracold Atoms (an NSF Physics Frontiers Center), the National Science Foundation, ARO MURI (W911NF2010082), DARPA ONISQ (W911NF2010021), and the DOE LBNL QSA Center (DE-AC02-05CH11231). B. G. acknowledges support from the DOD NDSEG. The device was fabricated at the Harvard CNS (NSF ECCS-1541959).

*These authors contributed equally to this work.
†Corresponding author: lukin@physics.harvard.edu

[1] N. P. de Leon, K. M. Itoh, D. Kim, K. K. Mehta, T. E. Northup, H. Paik, B. Palmer, N. Samarth, S. Sangtawesin, and D. Steuerman, Science **372**, eabb2823 (2021).
[2] C. Monroe and J. Kim, Science **339**, 1164 (2013).
[3] M. Saffman, T. G. Walker, and K. Mølmer, Rev. Mod. Phys. **82**, 2313 (2010).
[4] A. Browaeys and T. Lahaye, Nat. Phys. **16**, 132 (2020).
[5] S. Ebadi *et al.*, Science **376**, 1209 (2022).
[6] P. Huft, Y. Song, T. M. Graham, K. Jooya, S. Deshpande, C. Fang, M. Kats, and M. Saffman, Phys. Rev. A **105**, 063111 (2022).
[7] A. Reiserer and G. Rempe, Rev. Mod. Phys. **87**, 1379 (2015).
[8] T. Northup and R. Blatt, Nat. Photonics **8**, 356 (2014).
[9] W. Huie, S. G. Menon, H. Bernien, and J. P. Covey, Phys. Rev. Res. **3**, 043154 (2021).
[10] C. B. Young, A. Safari, P. Huft, J. Zhang, E. Oh, R. Chinnarasu, and M. Saffman, Appl. Phys. B **128**, 151 (2022).
[11] J. Ramette, J. Sinclair, N. P. Breuckmann, and V. Vuletić, arXiv:2302.01296.
[12] A. S. Sørensen, C. H. van der Wal, L. I. Childress, and M. D. Lukin, Phys. Rev. Lett. **92**, 063601 (2004).
[13] H. Kübler, J. Shaffer, T. Baluktsian, R. Löw, and T. Pfau, Nat. Photonics **4**, 112 (2010).
[14] J. A. Sedlacek, E. Kim, S. T. Rittenhouse, P. F. Weck, H. R. Sadeghpour, and J. P. Shaffer, Phys. Rev. Lett. **116**, 133201 (2016).
[15] G. Epple, K. S. Kleinbach, T. G. Euser, N. Y. Joly, T. Pfau, P. S. J. Russell, and R. Löw, Nat. Commun. **5**, 4132 (2014).
[16] K. S. Rajasree, T. Ray, K. Karlsson, J. L. Everett, and S. Nic Chormaic, Phys. Rev. Res. **2**, 012038(R) (2020).
[17] J. D. Carter and J. D. D. Martin, Phys. Rev. A **88**, 043429 (2013).
[18] D. Davtyan, S. Machluf, M. L. Soudijn, J. B. Naber, N. J. van Druten, H. B. van Linden van den Heuvell, and R. J. C. Spreeuw, Phys. Rev. A **97**, 023418 (2018).
[19] J. de Hond, R. van Bijnen, S. J. J. M. F. Kokkelmans, R. J. C. Spreeuw, H. B. van Linden van den Heuvell, and N. J. van Druten, Phys. Rev. A **98**, 062714 (2018).
[20] C. Hermann-Avigliano, R. C. Teixeira, T. L. Nguyen, T. Cantat-Moltrecht, G. Nogues, I. Dotsenko, S. Gleyzes, J. M. Raimond, S. Haroche, and M. Brune, Phys. Rev. A **90**, 040502(R) (2014).
[21] T. Thiele, S. Filipp, J. A. Agner, H. Schmutz, J. Deiglmayr, M. Stammeier, P. Allmendinger, F. Merkt, and A. Wallraff, Phys. Rev. A **90**, 013414 (2014).
[22] M. Kaiser, C. Glaser, L. Y. Ley, J. Grimmel, H. Hattermann, D. Bothner, D. Koelle, R. Kleiner, D. Petrosyan, A. Günther, and J. Fortágh, Phys. Rev. Res. **4**, 013207 (2022).
[23] T. G. Tiecke, J. D. Thompson, N. P. de Leon, L. R. Liu, V. Vuletić, and M. D. Lukin, Nature (London) **508**, 241 (2014).
[24] T. Đorđević, P. Samutpraphoot, P. L. Ocola, H. Bernien, B. Grinkemeyer, I. Dimitrova, V. Vuletić, and M. D. Lukin, Science **373**, 1511 (2021).
[25] G.-Q. Liu, Y.-R. Zhang, Y.-C. Chang, J.-D. Yue, H. Fan, and X.-Y. Pan, Nat. Commun. **6**, 6726 (2015).
[26] A. Cooper, W. Kyu Calvin Sun, J.-C. Jaskula, and P. Cappellaro, Phys. Rev. Appl. **12**, 044047 (2019).
[27] Z. Qiu, U. Vool, A. Hamo, and A. Yacoby, npj Quantum Inf. **7**, 39 (2021).
[28] J. Rovny, Z. Yuan, M. Fitzpatrick, A. I. Abdalla, L. Futamura, C. Fox, M. C. Cambria, S. Kolkowitz, and N. P. de Leon, Science **378**, 1301 (2022).
[29] V. Meyer, M. A. Rowe, D. Kielpinski, C. A. Sackett, W. M. Itano, C. Monroe, and D. J. Wineland, Phys. Rev. Lett. **86**, 5870 (2001).
[30] C. F. Roos, M. Chwalla, K. Kim, M. Riebe, and R. Blatt, Nature (London) **443**, 316 (2006).
[31] T. Ruster, H. Kaufmann, M. A. Luda, V. Kaushal, C. T. Schmiegelow, F. Schmidt-Kaler, and U. G. Poschinger, Phys. Rev. X **7**, 031050 (2017).
[32] T. Manovitz, R. Shaniv, Y. Shapira, R. Ozeri, and N. Akerman, Phys. Rev. Lett. **123**, 203001 (2019).
[33] B. C. Nichol, R. Srinivas, D. P. Nadlinger, P. Drmota, D. Main, G. Araneda, C. J. Ballance, and D. M. Lucas, Nature (London) **609**, 689 (2022).

[34] D. K. Shin, J. A. Ross, B. M. Henson, S. S. Hodgman, and A. G. Truscott, New J. Phys. **22**, 013002 (2020).
[35] L. Pezzè, A. Smerzi, M. K. Oberthaler, R. Schmied, and P. Treutlein, Rev. Mod. Phys. **90**, 035005 (2018).
[36] D. Bluvstein, H. Levine, G. Semeghini, T. T. Wang, S. Ebadi, M. Kalinowski, A. Keesling, N. Maskara, H. Pichler, M. Greiner, V. Vuletić, and M. D. Lukin, Nature (London) **604**, 451 (2022).
[37] See Supplemental Material at http://link.aps.org/supplemental/10.1103/PhysRevLett.132.113601 for technical details, including Refs. [38–40].
[38] I. S. Madjarov, J. P. Covey, A. L. Shaw, J. Choi, A. Kale, A. Cooper, H. Pichler, V. Schkolnik, J. R. Williams, and M. Endres, Nat. Phys. **16**, 857 (2020).
[39] P. Samutpraphoot, T. Đorđević, P. L. Ocola, H. Bernien, C. Senko, V. Vuletić, and M. D. Lukin, Phys. Rev. Lett. **124**, 063602 (2020).
[40] S. Weber, C. Tresp, H. Menke, A. Urvoy, O. Firstenberg, H. P. Büchler, and S. Hofferberth, J. Phys. B **50**, 133001 (2017).
[41] The Rydberg energy level u is typically notated as $u_{\mathbf{E}\neq 0} - u_{\mathbf{E}=0} = \Delta u = -\frac{1}{2}\alpha|\mathbf{E}|^2$ in an electric field $\mathbf{E}$. We instead plot the spectral shift ν where $\nu = -u$ and which is proportional to the electric field magnitude.
[42] M. S. O'Sullivan and B. P. Stoicheff, Phys. Rev. A **31**, 2718 (1985).
[43] H. Levine, A. Keesling, A. Omran, H. Bernien, S. Schwartz, A. S. Zibrov, M. Endres, M. Greiner, V. Vuletić, and M. D. Lukin, Phys. Rev. Lett. **121**, 123603 (2018).
[44] J. T. Wilson, S. Saskin, Y. Meng, S. Ma, R. Dilip, A. P. Burgers, and J. D. Thompson, Phys. Rev. Lett. **128**, 033201 (2022).
[45] L. Ma, E. Paradis, and G. Raithel, Opt. Express **28**, 3676 (2020).
[46] C. H. Bennett, G. Brassard, C. Crépeau, R. Jozsa, A. Peres, and W. K. Wootters, Phys. Rev. Lett. **70**, 1895 (1993).
[47] J. D. Thompson, T. G. Tiecke, N. P. de Leon, J. Feist, A. V. Akimov, M. Gullans, A. S. Zibrov, V. Vuletić, and M. D. Lukin, Science **340**, 1202 (2013).
[48] I. Cong, H. Levine, A. Keesling, D. Bluvstein, S.-T. Wang, and M. D. Lukin, Phys. Rev. X **12**, 021049 (2022).
[49] Y. Wu, S. Kolkowitz, S. Puri, and J. D. Thompson, Nat. Commun. **13**, 4657 (2022).
[50] J. D. Pritchard, J. A. Isaacs, M. A. Beck, R. McDermott, and M. Saffman, Phys. Rev. A **89**, 010301(R) (2014).
[51] Y. Liu, L. Li, and Y. Ma, Phys. Rev. Res. **4**, 013008 (2022).
[52] D. Petrosyan, G. Bensky, G. Kurizki, I. Mazets, J. Majer, and J. Schmiedmayer, Phys. Rev. A **79**, 040304(R) (2009).